RESEARCH ARTICLE

Health Risks and Toxicity of Zinc Oxide Nanoparticles in Rats: Assessment of Inflammatory and Oxidative Stress Effects

Rehab Ismail, Hisham Zaki[2], Hesham Saeed[1]*

[1] Department of Biotechnology, Institute of Graduate Studies and Research, Alexandria University
[2] Department of Environmental Studies, Institute of Graduate Studies and Research, Alexandria University
*Corresponding author: Hesham Saeed, hesham25166@alexu.edu.eg

Abstract

Zinc oxide (ZnO) nanoparticles are widely used in various medical and health products, including cosmetics, sunscreens, and antimicrobial agents. However, their potential toxicity raises significant concerns. This study investigates the in vivo toxicity of ZnO NPs using a rat model. Male Wistar rats were divided into four groups and treated intraperitoneally with different doses of ZnO NPs (50, 100, and 150 mg/kg) for three weeks, with a control group receiving normal saline. Post-treatment, rats were assessed for body weight changes, and were sacrificed for hematological, biochemical, and molecular analyses.

Findings revealed that ZnO NPs led to reduced weight gain and persistence in brain cells, particularly in lysosomes, as observed via transmission electron microscopy. Hematological analysis showed decreased RBC count, hemoglobin, MCH, and MCHC, with an increase in WBC count, indicating hematotoxicity. Hepatotoxicity was evident through reduced levels of ALT, AST, and ALP, along with increased oxidative stress markers. Neurotoxic effects were indicated by disrupted AChE activity and reduced Na+/K+ ATPase activity in brain mitochondria. Molecular analysis showed elevated pro-inflammatory mediators and disturbances in neurotransmission. These results highlight the potential toxicological impacts of ZnO NPs and stress the need for caution in their use.

Keywords: ZnO NPs; Toxicity ; Inflammation.

1. Introduction

Nanotechnology represents a groundbreaking platform with the potential to revolutionize biological, biochemical, and medical applications through novel uses and enhanced technologies. One key aspect driving this intense interest is the ability of nanotechnology to enable the controlled synthesis of materials with dimensions smaller than 100 nm. This ultra-small size is comparable to naturally occurring proteins and biomolecules in cells and is notably smaller than the diameter of many human cells [1].

Zinc oxide (ZnO) is one of the most widely used nanomaterials, with extensive applications in medicine and health-related products such as cosmetics, toothpastes, sunscreens, antimicrobial agents, deodorants, medical and sanitary materials, and over-the-counter topical products. ZnO is also emerging in new trends for medical imaging, advanced drug delivery systems, and selective destruction of tumor cells. Notably, ZnO nanoparticles (ZnO NPs) show promise as prophylactic agents for preventing HSV-1 and HSV-2 infections in vivo [2, 3].

Despite the growing body of literature on nanomaterials, the biological effects of ZnO NPs remain insufficiently understood and often controversial. Many in vitro studies suggest that ZnO toxicity involves the generation of reactive oxygen species (ROS), with enhanced dissolution of smaller particles playing a critical role [3, 4]. ZnO NPs can enter the bloodstream via inhalation, ingestion, or through damaged skin, subsequently being transported to various organs, including the brain, heart, liver, kidneys, spleen, bone marrow, and nervous system [5].

Special emphasis has been placed on the neurotoxic

potential of ZnO nanoparticles and their toxicity to glial cells. The discussion includes various factors contributing to the toxic potential of ZnO NPs and the cell signaling pathways involved in their toxicity. Current data suggest a risk associated with the uncontrolled use of zinc nanoformulations. With their increasing use, ZnO NPs present a significant threat to both the ecosystem and human health [6].

ZnO NPs have the potential to affect human neuron cells by crossing biological membranes, potentially leading to neurodegenerative diseases by altering specific cellular functions. They can impact parameters such as acetylcholinesterase (AChE), Na+/K+-ATPase, catalase, superoxide dismutase (SOD), and malondialdehyde (MDA) [5]. AChE is a crucial enzyme in the nervous system, rapidly hydrolyzing acetylcholine to choline and acetate, thus playing an essential role in cholinergic neurotransmission [7]. Na+/K+-ATPase, an enzyme located in the cell membrane, ensures the transmembrane transfer of Na+ and K+ ions, using ATP hydrolysis for energy [7]. Catalase protects cells from hydrogen peroxide's toxic effects and promotes cell growth [8]. SOD is a primary internal antioxidant defense, crucial for reducing oxidative stress [8, 9]. MDA, a product of lipid peroxidation, serves as a biomarker for oxidative stress in cells [10].

Imbalances in the antioxidant system have been associated with nanoparticle exposure (Diniz et al., 2013). High levels of reactive oxygen species (ROS) with ROS-scavenging enzymes, such as glutathione peroxidase (GPx), superoxide dismutase (SOD), and catalase (CAT). However, if these enzymes are overwhelmed by the excessive production of ROS, irreversible cellular damage and cell death may occur [10].

While the beneficial effects of ZnO NPs in nanomedicine are promising, their potential biological and environmental hazards must also be carefully considered.

2. Materials and Methods

2.1 Characterization of Zinc Oxide Nanoparticles

Zinc oxide nanoparticles (ZnO nps) were Purchased from Nanomaterials Co., USA. The physical properties of zinc oxide nanoparticles were characterized using Scanning Electron Microscope, Electron Microscope Unit, College of Science, Alexandria University, Alexandria, Egypt

2.2 Animals Groups and Treatments

Male rats weighing approximately 140-160 g were obtained from Egyptian Company for Serums, Vaccines and Medicines, Helwan, Cairo, Egypt. The animals were housed in cages (6 per cage) in

the animal house facilities located at the Institute of Graduate Studies and Research, Alexandria University. The animals fed a standard laboratory diet and water. The animals were kept under controlled hygienic conditions and maintained at a temperature 24 + 1oC with 50% humidity and time controlled lighting to a 12 h light/day. Rats were kept for two weeks for acclimation at room temperature before treatment. All rats were handled according to the standard guide for care and use of laboratory animals (OECD 1992 guidelines 407).The rats were divided into four groups 6 animals each. A control group received normal saline at dose of 1 mL/rat intraperitoneal three times per week. The second group was the zinc oxide nanoparticles low dose chronic group were received 50 mg/kg body weight of ZnONPs intraperitoneal three times per week and three weeks. Zinc oxide nanoparticles were prepared in normal saline and solubilized by sonication at room temperature for 30 minutes. A third group, the zinc oxide nanoparticles middle dose chronic group received 100 mg/kg body weight of ZnONPs intraperitoneal three times per week and three weeks. The fourth group, zinc oxide nanoparticles high dose chronic group received 120 mg/kg body weight of ZnONPs intraperitoneal for three times per week and for three weeks. The concentration of zinc oxide nanoparticles used in this study was determined from sublethal dose according to LD50 of zinc oxide nanoparticles mentioned in material safety data sheet and literature reviews. ZnONPs were dissolved in normal saline and by sonication. After treatment, the animals were sacrificed after being anesthetized with light ether. Liver and braint issues were rapidly removed from the animal groups and placed on ice. Small fractions from the brain tissues were removed immediately and immersed in RNA Later solution (Ambion, Courtier, France) and kept at 4 °C for overnight after which all samples are stored at -20 °C till used for RNA isolation and purification. Blood samples were also collected by direct heart puncture in heparin treated sterilized tubes.

2.3 Total Protein Determination by Lowry

Total protein was determined according to Lowry [11]. Lowry's reagent A, was freshly prepared by diluting Folin Ciocalteau's reagent (2N) to 1:1 with deionized water. Reagent B, 2% Na K tartarate.Lowry's reagent C, 1% CuSO4. Reagent D was prepared by dissolving 20 g of Na2CO3 in 0.1N NaOH then, the volume was adjusted to 1L in a volumetric flask. Reagent E was prepared by mixing one volume of reagent B plus one volume of reagent C. Finally, reagent F was prepared by mixing one volume of reagent E with 50 volume of reagent D. For each protein sample to be determined, 2.5 ml of reagent E was added, mixed

well and let to stand for 10 minutes at room temperature. After which, 0.25 ml of reagent F was added and mixed well and let to stand for 30 minutes at room temperature then, the absorbance was measured at 750 nm against a blank of 0.5 ml of sample buffer containing the same reagents previously described and under identical assay conditions. Bovine serum albumin (Sigma- Aldrich chemical Co, USA) was used as a standard at a concentration of 0.5 mg/ml.

2.4 Blood Hematology and Biochemical Characteristics

Blood samples collected in heparin-treated tubes were analyzed for hematological parameters Hb, hematocrite, packed cell volume (PCV), Red Blood Cells (RBCs) count and White Blood Cells (WBCs) count. Plasma was collected by centrifugation at 700xg for 20 minutes and stored at -80 °C.

Hemoglobin concentration was measured in the whole blood shortly after collection using Hb determination kit (Diamond Diagnostics Egypt). RBCs were counted on an AO bright line hemocytometer using a light microscope at 430 X magnification. Blood samples were diluted 200 times with physiological saline solution before counting. Microhematocrit tubes with a hematocrit centrifuge at a speed of 16,500 xg for 5 minutes were used to determine PCV. WBCs were counted on AO bright line hemocytometer using a light microscope at 100 X magnification after diluting blood samples 20 times with a diluting fluid containing, 1% acetic acid and a few microliters of Leshman's stain before counting. Blood indices were calculated according to Rahmanet al. [12] to determine the changes in red blood corpusles as follow; MCV (cu µ)= PCV (%) No. RBCs per 100 ml, MCH (pg)= Hb (gm per 100 ml)/ No. RBCs per 100 ml, and MCHC (%)= [Hb (gm per 100 ml)/PCV (%) x 100.

2.4.1 Assay of Aspartate Aminotransferase (AST)

AST was measured according to Reitman and Frankel (1957) [13]. The oxaloacetate which is formed in this enzymatic reaction was measured by adding 2,4-dinitrophenylhydrazine which yield a reddish-brown color in an alkaline medium. The incubation reaction contained 0.5 mL of AST substrate (0.1 M phosphate buffer pH 7.5, 0.002 M α-oxoglutarate and 0.2 M L-aspartic acid). The protein samples of 0.1 ml were then added and the reactions proceeded at 37 °C for 60 minutes. Color forming reagent, 2,4-dinitrophenylhydrazine, was then added and the reaction tubes were left for 20 minutes at room temperature after which the alkaline reagent, 0.4 N NaOH was then added and left for 5 minutes. The absorbance was then read at 505 nm against a blank solution containing distilled water.

2.4.2 Assay of Aspartate Aminotransferas (AST)

ALT was measured according to Reitman and Frankel [13]. Pyruvate which is formed was measured photometrically after the addition of 2,4-dinitrophenylhydrazine which gave a reddish brown color in alkaline medium at a wavelength of 505 nm. The reaction mixture contained 0.5 mL of ALT substrate (0.1 M phosphate buffer pH 7.5, 0.002 M α-oxoglutarate and 0.2 M dL-alanine). This mixture was incubated at 37 °C for 5 minutes followed by the addition of 0.1 mL of sample after which the reaction was continued for 60 minutes at 37 °C. Color-forming reagent (2,4-dinitrophenylhydrazine) was then added and left for 20 minutes at room temperature after which alkaline reagent 0.4 N NaOH was added and left for additional 5 minutes. The absorbance was read at 505 nm against blank solution containing distilled water.

2.4.3 Assay of Alkaline Phosphatase (ALP)

ALP was measured according to Belfield & Goldberg [14]. The reaction mixture contained 0.5 Ml of 50 mM phosphate buffer, pH 10.0 and 5 mM phenylphosphate and 0.025 ml of protein samples. The reaction mixture was incubated at 37 °C for 20 minutes after which the reaction was terminated by the addition of 100 mM EDTA and 50 mM 4-aminophenazone. Color-forming reagent composed of 200 mM potassium ferricyanide was then added to the reaction tube, mixed well and stood for 5 minutes at room temperature in a dark place. The liberated -nitrophenol was then measured spectrophotometrically. One mL of working reagent, 10 mLof buffering reagent contained, 0.9 M/L 2,4-amino-2-methyl-1-propanol buffer pH 10.5 and 2 mM magnesium sulfate to substrate reagent, 5.5 M 2,4-nitrophenylphosphate. This mixture was incubated at 37 °C for 30 minutes after which the alkaline reagent, 10 mL of 0.4 N NaOH was then added and the absorbance was read at 510 nm. One unit of enzyme activity was the amount of enzyme that liberates one micromole of phenol per minute at the indicated temperature.

2.4.4 Assay of Acetylcholinesterase (AChE) in Brain

Brain tissue was homogenized in a glass Teflon homogenizer in a buffer solution containing 0.25 M sucrose, 1% Triton-X100 in 0.1 M phosphate buffer pH 7.4 in a ratio of 1:3 (brain tissue weight: buffer). After homogenization, filtration was carried out through double sheath cloth after which centrifugation was done at 10,000 xg for 10 minutes. The supernatant was collected, aliquots and stored at -80 °C until it was used for acetylcholinesterase assay.

Acetylcholinesterase activity was measured according to Ellman et al [15]. The assay depends

mainly on the formation yellow color produced by thiocholine when reacts with dithiobis-2-nitrobenzoate (DTNB) ion. The reaction mixture contained 750 µl of 0.1 M phosphate buffer pH 7.4, 25 µl DNTB and 100 µl brain tissue homogenate. The reaction tubes were then shaken and the absorbance of the yellow color produced was measured spectrophotometrically at 412 nm previously adjusted to zero using a blank containing all of the reagent mix except the enzyme. 25 µl of 0.075 M acetylcholine iodide was added gently to ensure thoroughly mixing and the absorbance was measured every 30 seconds over 7 minutes. Specific activity was expressed as µmoles product formed per minute per mg protein using a molar extinction coefficient of the adduct formed between thiocholine and DTNBas 13.6 µM -1 cm -1.

2.5 Assay of Adenosine Triphosphatase (ATPase)

Isolation of mitochondria from the brain tissue

Mitochondria were prepared according to Koch.[16]. Brain tissues were dissected and placed on ice cold medium containing 0.25 M sucrose, 1 mM EDTA, and 20 mM Tris-HCl, pH 7.4 and homogenized with Teflon homogenizer for 30 seconds. The brain homogenate was filtered through a double layer of cheese cloth after which centrifugation was carried out at 750 xg for 10 minutes at 4 °C using high-speed centrifuge Beckman Model J 2-21. The supernatant fraction was collected and centrifuged at 9000 xg for 10 minutes at 4 °C to give a mitochondrial pellet. The mitochondrial pellet was resuspended in 0.25 M sucrose and stored at -20 °C until used for the assay.

2.5.1 Assay of Mitochondrial brain Na+/K+ ATPase

Brain mitochondrial Na^+/K^+ ATPase activity was determined using the endpoint of phosphate analysis following the method of Taussky & Shorr [17]. A 1.0 ml reaction mixture contained 5 mM ATP, 5 mM $MgCl_2$, 100 mM NaCl, 20 mM KCl, 135 mM imidazole/HCl buffer, pH 7.5 and 35-40 µg of enzyme. The reaction was initiated by the addition of the mitochondrial fraction and allowed to proceed for 30 minutes with constant shaking at 37 °C. After the incubation period, the reaction was terminated by the addition of 0.1 mL of 50% ice-cold TCA. The total ATPase activity was measured in the presence of Na^+, K^+, and Mg^{+2} ions in the reaction mixture. The Mg^{+2} ATPase was measured in the presence of 1 mM oubain, a specific inhibitor for Na^+/ K^+ ATPase. Na^+/ K^+ ATPase was determined as the difference between total and Mg^{+2} ATPase. Inorganic phosphate was estimated in each supernatant fraction and the absorbance obtained was compared to a standard curve of known Na_2HPO_4 concentrations between 0.1-1 µmoles/ml

2.6 Determination of Glutathione S-transferase (GST)

Glutathione S-transferase activity in the liver homogenate was measured according to the method of Habig et al. [8]. The reaction mixture contained 30 µg protein of the supernatant fraction, 0.5 mL reduced glutathione (0.5 mM) and 0.1 mL sodium phosphate buffer pH 7.3. Preincubation was carried out for 5 minutes at 37 °C followed by the addition of 50 µl of 1-chloro-2,4-dinitrobenzene (CDNB, 0.5 mM) and incubation was continued for 5 minutes at 37 °C. The reaction was terminated by the addition of 0.2 mL of 33% TCA. Centrifugation was carried out for 5 minutes at 3000 rpm and CDNBconjugate was measured spectrophotometrically at 340.

2.7 Measurement of Reduced Glutathione

Reduced glutathione was measured in rat liver homogenate according to Beutler et al. [19] utilizing a commercial kit obtained from Biodiagnostics Co., Egypt. The method based on the reduction of 5,5'-dithiobis (2-nitrobenzoic acid) (DTNB) with glutathione (GSH) to produce a yellow compound. The reaction was done by adding 0.5mL of liver homogenate with 0.5ml TCA, mixing and centrifuged at 3000 rpm for 15min. 0.5mL of supernatant was added to 0.1mL DTNB in 0.5mL reaction buffer, mixed well and the absorbance was measured at 405 nm. The reduced chromogen is directly proportional to GSH concentration at 405 nm.

2.8 Assay of Catalase

Catalase was measured in rat liver homogenate according to Aebi et al. and Fossati et al. [20, 21] utilizing a commercial kit obtained from Biodiagnostics Co., Egypt. One unit of catalase is the amount of enzyme that decomposes 1 µM of H_2O_2/minute at 25 °C and pH 7.0. Catalase reacted with a known concentration of H_2O_2 for one minute after which the reaction was terminated by the addition of a catalase inhibitor. In the presence of horse radish peroxidase (HRP), the remaining H_2O_2 reacted with 3,5-dichloro-2-hydroxybenzene sulfonic acid (DHBS) and 4-aminophenazone (AAP) to form a chromophore with color intensity inversely proportional to the amount of catalase present in the original sample.

2.9 Assay of Glutathione Peroxidase

Glutathione peroxidase activity (GPx) was measured according to Paglia and Valentine (1967) [22] utilizing a commercial kit obtained from Biodiagnostics, Egypt. The principle of the assay is an indirect measurement of the activity of c-GPx, oxidized glutathione (GSSG) is produced upon the reduction of an organic peroxide by c-GPx, is

recycled to its reduced state by enzyme glutathione reductase (GR).

The oxidation of NADPH to $NADP^+$ is accompanied by a decrease in absorbance at 340 nm providing a spectrophotometric means for monitoring GPx enzyme activity. The reaction mixture contained 1 ml 50 mM phosphate buffer, Triton-X100, pH 7.0), 0.1 ml NADPH 24 µM and 0.01 ml of the liver homogenate. The reaction is started by adding 0.01 ml diluted hydrogen peroxide and the decrease in the absorbance was recorded at 340 nm over 3 minutes. Enzyme activity was determined using a molar extinction coefficient of NADPH 6220 $M^{-1} cm^{-1}$. The rate of decrease in the absorbance is directly proportional to the GPx activity in the sample.

2.10 Assay of Thiobarbituric acid Reactive Substances (TBARS)

Thiobarbituric acid reactive substances were measured as described by Tappel & Zalkin. [23] One mL of homogenate was added to 2mL of 7.5% trichloroacetic acid and mixed well after which centrifugation was carried out at 1000 xg for 10 minutes and 2mL of the supernatant was added to 1Ml of 0.7% 2-thiobarbituric acid. After boiling for 10 minutes the reactants were cooled and TBARS were measured at 532 nm. An extinction coefficient of 156,000 $M^{-1} cm^{-1}$ was used for calculations.

2.11 Isolation of Total RNA from Brain Tissue for Determination of Gene Expression

Frozen reserved brain tissues were retrieved from the RNA later solution and left on ice to be completely thawed. Brain tissue samples, 60 mg each, were then homogenized in RNA lysis solution. After complete lysis of the tissue samples, 350 µl of RNA dilution buffer was added to each samples and mixed well by inverting the tubes 4-5 times then tubes were heated at 70 °C for 30 minutes. The tubes were then centrifuged at 13,000 rpm for 10 minutes at 4 °C after which the clear lysates were transferred to afresh sterilized tubes and 200 µl of 95% ethanol was added to each tube and mixed thoroughly. The mixture was transferred to a spin column assembly and centrifugation was carried out at 13,000 rpm for 1 minute at 4 °C. The eluate was discarded and 750 µl of RNA washing solution was added and centrifugation was carried out for 1 minute at 13,000 rpm at 4 °C. To each spin column, a DNase solution mix containing yellow core buffer and magnesium chloride at a concentration of 0.09 M is added carefully followed by incubation at room temperature for 15 minutes to hydrolyze genomic DNA. The reactions were terminated by the addition of 200 µl of DNase stop solution and centrifuged for 1 minute at 13,000 rpm at 4 °C. Columns containing bounded total RNA were then washed two times with 750 µl RNA washing solution as described earlier. Bound total RNA was then eluted by adding 100 µl of nuclease-free water followed by centrifugation for 1 minute at 13,000 rpm at 4 °C. The purity and the concentration of RNA samples were determined spectrophotometrically by measuring the absorbance at 260 and 280 nm. One absorbance unit at 260 nm is equivalent to 40 µg RNA per mL

2.12 Real Time PCR Expression SYBR Green

Gene expression levels were measured by real time PCR using SYBR Green master mix provided by Jena Bioscience, Germany, and using Qiagene® Rotor gene PCR machine instrument located at the Central Laboratory at the Institute of Graduate Studies and Research. SYBR Green master is designed for quantitative real-time analysis of DNA samples using fluorescent DNA stain EvaGreen®. The fluorescent dye in the master mix intercalates into the amplification product during the PCR process and enables the rapid analysis of target DNA without the need to synthesize sequence-specific labeled probes. The mixture contained qPCR polymerase, dATP, dCTP, dUTP, dGTP, Evagreen dye, reaction buffer with KCl, ammonium sulfate, magnesium chloride and stabilizers. The reaction mixtures contained 10 µl qPCR green master mix, 2 µl of forward and reverse primers, 5 µl of 1 to 5 diluted cDNA and 4 µl of nuclease-free distilled water. The mixtures were mixed thoroughly to ensure homogeneity and finally spin down to collect the solution mix. The real time PCR conditions were as follows, initial denaturation at 95 °C for 5 minutes followed by 40 cycles for 30 seconds at 95 °C, annealing and elongation for 1 minute at 60 to 65 °C according to the primers melting temperature one cycle at 95 °C for 1 minute.After the end of the run CT values (threshold cycle value) were analyzed manually at a factor of 0.04. Amplification and melting curves and CT values were collected for statistical analysis of the results.The expression of targeted genes was normalized to the reference gene β-actin expression levels within the same sample to determine ΔCT. This step serves to correct for non-treatment-related variation among wells such as potential differences in cell number. ΔCT was then normalized to the expression of the targeted gene in treated animals from a separate untreated sample to find ΔΔCT. % Expression was calculated by the equation (%Expression = $2^{-\Delta\Delta CT}$). PCR Primers used in this study: β-actine; FWD 5'- TAC AAC CTC CTT GCA GCT CC -3', REV 5'- GGA TCT TCA TGA GGT AGT CAG TC -3' Tyrosine Hydroxylase(TH) FWD 5'TACCTCCGGGTGACAGCATA -3', REV 5'GGGCTGTGGAGACAGAACTC -3', Monocyte Chemoattractant Protein (MCP); FWD5'-CTGTAGCATCCACGTGCTGT -3', REV 5'GGTGCTGAAGTCCTTAGGGT -3', Vesicular

Monoamine Transferase (VMT); FWD 5'TCACTGTGGTGGTGTTTGCT-3', REV 5'-ATTCCCATGGCTCTCCCTCT -3' , Inducible Nitric Oxide Synthase (iNOS); FWD 5'GCCCAACAACACAGGATGAC-3' REV 5'CCTTGTGGTGAAGGGTGTCG-3'

2.12 *Statistical Analysis*

The data were analyzed using GraphPad Prizm7 2016. The significance of the differences was calculated using one-way ANOVA followed by Dunnett's test for multiple comparisons. $P < 0.05$ was considered statistically significant.

3. Results

3.1 *Characterization of Zinc Oxide Nanoparticles using Scanning Electron Microscope*

From the analysis of the scanning electron micrograph zinc oxide nanoparticles are nearly spherical and quite monodisperse. However, there are some larger aggregates in the sample because of the high surface energy of ZnO nanoparticles that results in aggregation. The synthesized particle diameter ranges between 35 and 45 nm for the material tested fig 1.
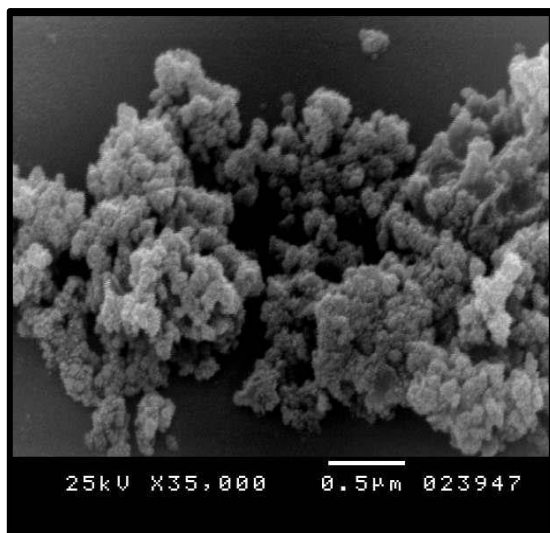

Figure 1. Scanning electron micrograph showing zinc oxide nanoparticles spheres with average size 35-45 nm**.**

3.2 *Biodistribution and Accumulation of Zinc Oxide Nanoparticles in Brain Cells*

By using TEM to investigate whether ZnO-NPs had entered the brains of exposed rats. Samples of ZnO-NP-exposed and control brains were compared. Figure 5 shows that section from ZnO-NP-exposed rats exhibit numerous black spots which are not found in section from control rat brains figure 2. Those black spots indicate penetration of ZnO NPs to brain cells which mainly accumulated in lysosomes fig 2.
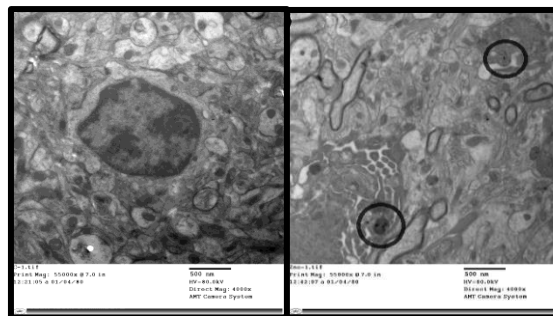

Figure 2. Transmission electron micrograph showing brain cells from zinc oxide nanoparticles treated rats in which zinc oxide nanoparticles appear to be accumulated in lysosomes (bold circles).

3.3 *Effect of Different Doses of Zinc Oxide Nanoparticles on Body Weight of Treated Male Rats*

No death was observed in any of the experimental groups. A significant reduction was detected in body weight gain in both middle-dose and high-dose chronically treated groups treated groups compared to the control group. The changes in body weight throughout the experimental period are presented in Table 1 The study examined the impact of chronic exposure to zinc oxide nanoparticles (ZnO NPs) on the body weight of male Wistar rats over three weeks. Four groups were established: a control group treated with normal saline, and three treatment groups receiving low (50 mg/kg/day), medium (100 mg/kg/day), and high (150 mg/kg/day) doses of ZnO NPs. The control group exhibited significant weight gain, with final body weights averaging 200 g, indicating normal growth. In contrast, the low-dose group showed less weight gain, with final body weights averaging 180 g, suggesting that even low doses of ZnO NPs can impede growth. The medium-dose group had a more pronounced reduction in weight gain, averaging 135 g, highlighting a stronger toxic effect at this dosage. The high-dose group experienced the most severe impact, with final body weights averaging 130 g, indicating significant adverse health effects at higher dosages.

Table 1: Changes in body weight (gm) of male rats treated with different doses of zinc oxide nanoparticles

Group	Initial body weight (IBW)	Final body weight (FBW)
Control	150± 10	200±5 a
Low chronic dose (50mg/kg/day)	150± 10	180±5 d
Middle chronic dose (100mg/kg/day)	150± 10	135±5 d
High chronic dose (150mg/kg/day)	150± 10	130±5 d

[abcd]Means within columns with different superscript are significantly differ (P<0.05)

3.3 Dose-Dependent Hematological Effects of Zinc Oxide Nanoparticles in Male Wistar Rats

The presented graph (figure 3] illustrates the hematological parameters of male Wistar rats subjected to different doses of zinc oxide nanoparticles (ZnO NPs) over a three-week period. The parameters measured include total leukocyte count (TLC), total erythrocyte count (TEC), hemoglobin (Hb), hematocrit (HCT), mean corpuscular volume (MCV), mean corpuscular hemoglobin (MCH), and mean corpuscular hemoglobin concentration (MCHC).

In the control group, TLC, TEC, Hb, HCT, MCV, MCH, and MCHC values fall within normal ranges, indicating typical physiological conditions. The low chronic dose group (50 mg/kg/day) shows a significant increase in TLC compared to the control, suggesting an inflammatory or immune response, while TEC, Hb, HCT, MCV, MCH, and MCHC levels remain relatively unchanged, indicating minimal hematotoxic effects at this dose.

The medium chronic dose group (100 mg/kg/day) exhibits a marked increase in TLC and a significant reduction in TEC, Hb, and HCT levels, indicating substantial hematotoxicity. This group also shows decreased MCH and MCHC values, reflecting potential disruptions in red blood cell (RBC) integrity and hemoglobin content.

In the high chronic dose group (150 mg/kg/day), the TLC is significantly elevated, indicating a robust inflammatory response.

This group also shows the most pronounced reductions in TEC, Hb, HCT, MCH, and MCHC levels, underscoring the severe hematotoxic effects of ZnO NPs at this dosage. The MCV remains relatively stable across all groups, suggesting that the size of RBCs is not significantly affected by ZnO NPs exposure.

Overall, these results highlight a dose-dependent hematotoxic effect of ZnO NPs, with higher doses causing significant disruptions in hematological parameters, which could lead to serious health implications.
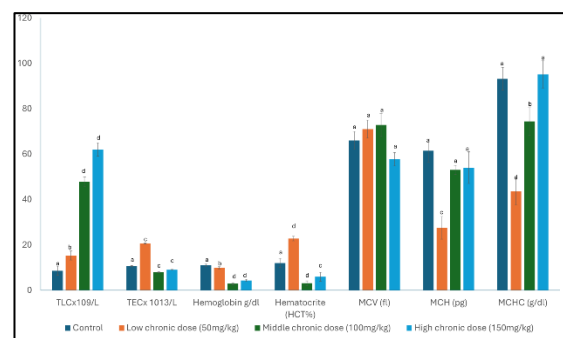

Figure 3. Dose-Dependent Hematological Effects of Zinc Oxide Nanoparticles. [abcd]Means within columns with different superscript are significantly different (P<0.05).

3.4 Effects of ZnO Nanoparticles Exposure on Liver Enzymes, Antioxidant Enzymes and Oxidative Stress Markers

The bar graph fig 4 illustrates the effects of varying chronic doses of ZnO nanoparticles on several biochemical parameters compared to a control group. The parameters measured include GST Activity, GPx Activity, GSH levels, Catalase Activity, AST, ALT, ALP, and TBARS concentration.

For GST Activity, the control group exhibited the highest activity at approximately 180 x 100 U/g. The low, middle, and high chronic doses resulted in lower activities of about 120, 130, and 140 x 100 U/g, respectively. GPx Activity was lowest in the control group at about 10 U/g, with a marked increase to around 150 U/g in the low dose, 140 U/g in the middle dose, and 130 U/g in the high dose groups, suggesting an induction of GPx activity with increasing doses of ZnO nanoparticles. GSH levels were highest in the control group at approximately 180 mmol/L, with significant reductions to around 120, 130, and 130 mmol/L in the low, middle, and high dose

groups, respectively. Catalase activity was notably higher in the control group at about 850 U/L, compared to the treated groups which showed similar levels around 700 U/L.

AST levels were considerably lower in the control group at around 40 U/L, compared to the treated groups, which had levels of about 80, 70, and 70 U/L for the low, middle, and high dose groups, respectively. ALT levels in the control group were about 25 U/L, while the treated groups exhibited higher levels of approximately 60 U/L across all doses. ALP levels were also lower in the control group at around 50 U/L, compared to the treated groups with levels around 130, 120, and 120 U/L for the low, middle, and high doses, respectively. TBARS concentration, an indicator of lipid peroxidation, was lowest in the control group at about 0.5 nmol/ml, with higher levels of around 1.5, 1.4, and 1.3 nmol/ml observed in the low, middle, and high dose groups, respectively, suggesting increased oxidative stress with higher doses.
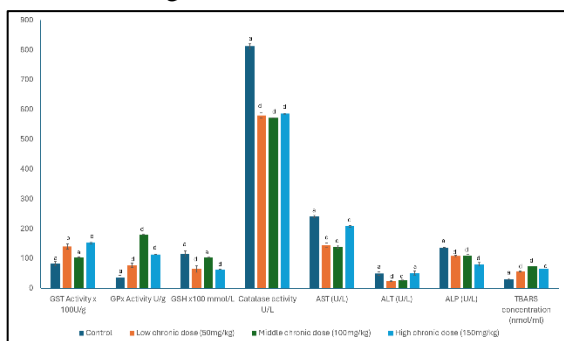

Figure 4. Effects of ZnO Nanoparticles Exposure on Liver Enzymes, Antioxidant Enzymes and Oxidative Stress Markers. [abcd]Means within columns with different superscript are significantly different (P<0.05).

3.5 Impact of Exposure to ZnO Nanoparticles on Various Brain Proteins and Their Activity

The bar graph fig 5 depicts the impact of varying chronic doses of ZnO nanoparticles on several biochemical parameters compared to a control group. The parameters measured include total protein content, acetylcholinesterase (AchE) specific activity, total mitochondrial protein, Na+/K+ ATPase activity, and Na+/K+ ATPase specific activity.

For total protein content, the control group showed a level of approximately 11 mg/ml. The low, middle, and high chronic doses

resulted in protein contents of about 10, 11, and 9 mg/ml, respectively. AchE specific activity was around 7 µmoles/min/mg protein in the control group. This activity decreased in the treated groups to about 3, 4, and 3 µmoles/min/mg protein for the low, middle, and high doses, respectively. Total mitochondrial protein content was highest in the control group at around 11 mg/ml, while the treated groups exhibited levels of about 8, 7, and 8 mg/ml for the low, middle, and high doses, respectively.

Na+/K+ ATPase activity was significantly higher in the control group at approximately 33 nmole/ml. The activity decreased in the treated groups to around 24, 20, and 21 nmole/ml for the low, middle, and high doses, respectively. Similarly, Na+/K+ ATPase specific activity was highest in the control group at about 23 µmol Pi/mg protein/min. The treated groups showed reduced specific activities of around 10, 12, and 16 µmol Pi/mg protein/min for the low, middle, and high doses, respectively.

Exposure to ZnO nanoparticles appears to reduce total protein content, AchE specific activity, total mitochondrial protein, and Na+/K+ ATPase activity and specific activity, indicating potential disruptions in biochemical functions at higher exposure levels.
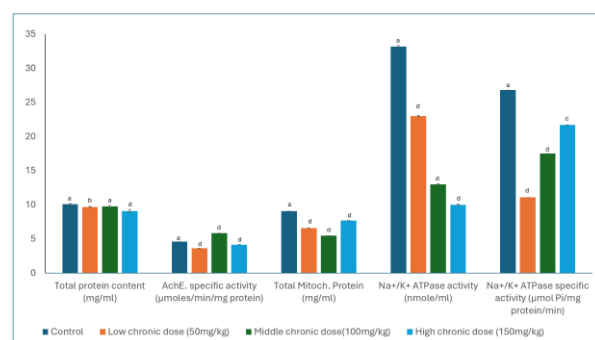

Figure 5. Effect of Exposure to ZnO Nanoparticles on various brain proteins and their activity

3.6 Proteins Transcription levels alterations upon Exposure to ZnO Nanoparticles

The bar graph fig 6 depicts the real-time expression levels of inducible nitric oxide synthase (iNOS), tyrosine hydroxylase (TH), monocyte chemoattractant protein (MCP), and vesicular monoamine transporter (VMAT) upon exposure to varying chronic doses of ZnO nanoparticles compared to a control group.

For iNOS, the control group exhibited an expression level of approximately 1.0. The exposure to low, middle, and high chronic doses of ZnO nanoparticles resulted in similar expression levels of around 1.2. This indicates a slight increase in iNOS expression with ZnO nanoparticle exposure, suggesting that these nanoparticles may induce a mild inflammatory response.

Regarding TH, the control group showed expression levels of about 2.7. In contrast, the treated groups (low, middle, and high doses) demonstrated similar expression levels of around 2.8 to 2.9. This consistent, slight increase in TH expression upon ZnO nanoparticle exposure implies that these nanoparticles might enhance the synthesis of catecholamines, as TH is a critical enzyme in this biosynthetic pathway.

For MCP, the control group had expression levels of approximately 1.0. The low, middle, and high chronic doses led to increased MCP expression levels of about 1.5, 1.6, and 1.5, respectively. This moderate increase in MCP expression with increasing doses of ZnO nanoparticles indicates that these nanoparticles could stimulate the recruitment of monocytes, thereby promoting inflammatory processes.

Lastly, VMAT expression levels in the control group were around 0.7. The treated groups exhibited lower expression levels of about 0.3, 0.4, and 0.5 for the low, middle, and high doses, respectively. This dose-dependent decrease in VMAT expression upon ZnO nanoparticle exposure suggests that these nanoparticles might impair the transport and storage of neurotransmitters in vesicles, potentially affecting neurotransmission.

Overall, the data suggest that chronic exposure to ZnO nanoparticles affects the expression levels of these proteins. There is a slight increase in iNOS and TH expression, a moderate increase in MCP expression, and a notable decrease in VMAT expression. These changes indicate that ZnO nanoparticles may influence inflammatory responses, neurotransmitter synthesis, and cellular stress responses.
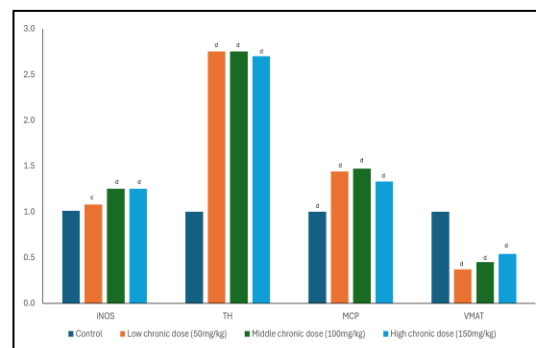

Figure 6. The effect (Log2, fold change) of ZnO nanoparticles different doses on *iNOs*, *TH*,

4. Discussion

Variety of the synthesis routes for ZnO NPs is remarkable [24-26]. However, it is still challenging to control their crystalline structure, stability, and dispersibility in common solutions such as water and ethanol [27,28] the complexity of synthetic reactions increases, a thorough understanding of the nanoparticle formation mechanism is needed [28, 29]. Control of ZnO NP stability, solubility, surface structure, shape, and aggregation properties represent some of the key roles for ZnO NP industrial and other practical applications [30]. As nano-industry develops, long-standing and traditional interpretations of particle formation mechanisms must be revisited.

Zinc oxide nanoparticles used in our study are nearly spherical particle diameters between 35 and 45 nm. This is consistent with the Literature indicating that the majority of as-synthesized ZnO nanoparticles do not show agreement between the crystallite size determined by XRD and the particle size determined by SEM/TEM. This discrepancy is likely due to the agglomeration of ZnO nanoparticles, which results in the particle size being larger than the crystallite size [31].

Transmission Electron Microscopy (TEM) was employed to assess the entry and distribution of ZnO nanoparticles (ZnO-NPs) in the brains of exposed rats. The TEM images reveal numerous black spots in the brain sections of ZnO-NP-exposed rats, which are absent in the control brain sections.

The accumulation of ZnO-NPs brain is consistent with growing evidence suggesting that ZnO nanoparticles can traverse biological barriers and reach the brain following oral ingestion. This is a significant finding given the increasing use of ZnO-NPs in various applications, including medical, cosmetic, and industrial products. Despite the widespread use, the neurotoxicity of ZnO-NPs after oral exposure remains insufficiently explored [32].

Our findings align with previous studies indicating

that nanoparticles, due to their small size and high surface area, can bypass the blood-brain barrier (BBB). Once in the brain, they can accumulate in various cell types, including neurons and glial cells. The observed accumulation in lysosomes suggests that these organelles may play a role in the cellular handling and potential sequestration of ZnONPs [33].

The neurotoxic effects of ZnO-NPs can be attributed to several mechanisms. One primary concern is the generation of reactive oxygen species (ROS), which can overwhelm the brain's antioxidant defenses, leading to oxidative stress [34].

Moreover, the ability of ZnO-NPs to induce inflammation in the brain further exacerbates their neurotoxic potential. Inflammatory responses can lead to the release of cytokines and other mediators that may cause additional neuronal damage and dysfunction. The accumulation in lysosomes suggests a disruption in normal cellular processes, as these organelles are crucial for waste degradation and recycling of cellular components.

In conclusion, the TEM analysis provides compelling evidence of ZnO-NP penetration and accumulation in rat brain cells, primarily within lysosomes. These findings underscore the need for further research to elucidate the full spectrum of neurotoxic effects associated with ZnO-NP exposure. Understanding these mechanisms is crucial for developing safer nanomaterials and establishing guidelines for their use to minimize potential risks to human health and the environment. This oxidative stress can damage cellular components, including lipids, proteins, and DNA, potentially resulting in cell death and contributing to neurodegenerative processes. Our study specifically focused on oxidative stress markers and antioxidant enzymes, as well as oxidative stress protein markers, to better understand the extent and implications of ZnONP-induced oxidative stress in brain cells.

he results of this study clearly illustrate the dose-dependent negative impact of zinc oxide nanoparticles (ZnO NPs) on body weight in rats. The control group exhibited significant weight gain, with final body weights indicating normal growth. This contrasts sharply with the ZnO NP- exposed groups, where even low doses of ZnO NPs impeded weight gain, as evidenced by the lower final body weights.

Specifically, the low-dose group showed less weight gain, suggesting that even minimal exposure to ZnO NPs can disrupt normal growth processes. The medium-dose group exhibited a more pronounced reduction in weight gain, highlighting a stronger toxic effect at this dosage. The high-dose

group experienced the most severe impact, with markedly lower final body weights, indicating significant adverse health effects at higher dosages.

These findings suggest that ZnO NPs interfere with normal metabolic processes, potentially leading to serious health issues, particularly at higher doses. The observed dose-dependent reduction in body weight gain underscores the importance of considering the potential risks associated with ZnO NP exposure. Further studies are needed to elucidate the mechanisms by which ZnO NPs exert these effects and to explore the long-term implications of their use in various applications.

In a previous range-finding study, rats exposed to a 14-day repeated oral dose of ZnONPs showed a decrease of body. Death was also observed in two male rats exposed to 2,000 mg/kg/day group [36].

Haematological evaluation of the studied groups included total leukocyte count (TLC), total erythrocyte count (TEC), hemoglobin (Hb), hematocrit (HCT), mean corpuscular volume (MCV), mean corpuscular hemoglobin (MCH), and mean corpuscular hemoglobin concentration (MCHC).

The low chronic dose group (50 mg/kg/day) shows a significant increase in TLC compared to the control, suggesting an inflammatory or immune response. However, TEC, Hb, HCT, MCV, MCH, and MCHC levels remain relatively unchanged, indicating minimal hematotoxic effects at this dose.

The medium chronic dose group (100 mg/kg/day) exhibits a marked increase in TLC and a significant reduction in TEC, Hb, and HCT levels, indicating substantial hematotoxicity. Additionally, this group shows decreased MCH and MCHC values, reflecting potential disruptions in red blood cell (RBC) integrity and hemoglobin content. A recent study showed a significant increase in neutrophil count observed in the group exposed to 100 mg/kg body weight (9.35 K/μL in Group 4 vs. 8.93 K/μL in the control group), suggesting a dose-dependent response [37]. Other studies have reported cytotoxic effects, including hemolysis and alterations in RBC morphology, upon exposure to ZnO nanoparticles [19,20].

The high chronic dose group (150 mg/kg/day) shows the most pronounced effects, with a significantly elevated TLC indicating a robust inflammatory response. This group also demonstrates the most severe reductions in TEC, Hb, HCT, MCH, and MCHC levels, underscoring the severe hepatotoxic effects of ZnO NPs at this dosage. Notably, the MCV remains relatively stable across all groups, suggesting that the size of RBCs is not significantly affected by ZnO NP exposure.

These results indicate that ZnO NPs induce dose-

dependent hematotoxicity, with higher doses causing significant disruptions in both white and red blood cell parameters. The marked inflammatory response and compromised RBC integrity at higher doses highlight the potential health risks associated with ZnO NP exposure.

The impact of various chronic doses of zinc oxide nanoparticles (ZnO NPs) was evaluated on several biochemical parameters, including liver enzymes, antioxidant enzymes, and oxidative stress markers, compared to a control group.

Glutathione S-transferase (GST) Activity: Control group exhibited the highest GST activity, indicating normal liver function. In contrast, the low, middle, and high chronic dose groups showed decreased GST activity, suggesting compromised liver detoxification processes3-L1 cells. . This is consistent study done by Pandurangan *et.al,* [40] to determine the effect of ZnO nanoparticles on the C2C12 and 3T3-L1 cell viability showed that ZnO nanoparticles increased antioxidant enzyme activities and their mRNA expression in the C2C12 and 3T

Glutathione Peroxidase (GPx) Activity: The control group had the lowest GPx activity, while the treated groups showed significantly increased GPx activity, indicating an upregulation of antioxidant defense mechanisms in response to ZnO NP exposure.The same results were obtained in a study done by Trevisan, R., *et al.,* about the toxicity of zinc oxide nanoparticles (ZnONP) in Pacific oysters *Crassostrea gigas* showed an increased index of lipid peroxidation and GPx activity [41].

Glutathione (GSH) Levels: The highest GSH levels were observed in the control group, with significant reductions in the treated groups. This decrease indicates a depletion of GSH, a critical antioxidant, due to oxidative stress induced by ZnO NPs. Akhtar M.J., *et.al.,*[42] reported that, ZnO NPs significantly altered the oxidant/antioxidant status of human liver cancer cells.

Catalase Activity: Catalase activity was notably higher in the control group, while the treated groups exhibited lower but similar levels, suggesting that ZnO NP exposure impairs the activity of this key antioxidant enzyme. This is of enormous importance as Catalase has one of the highest turnover rates for all enzymes: one molecule of catalase can convert approximately 6 million molecules of hydrogen peroxide to water and oxygen each minute [44].

Aspartate Aminotransferase (AST) and Alanine Aminotransferase (ALT) Levels: Both AST and ALT levels were considerably lower in the control group. The elevated levels in the treated groups indicate liver damage and hepatotoxicity caused by ZnO NPs. According to *Sharma et al.,* 2012 [43,

44] a significant accumulation of nanoparticles in the liver le to cellular injury after sub-acute oral exposure of ZnO nanoparticles (300 mg/kg) for 14 consecutive days. This was evident by the elevated alanine aminotransferase (ALT) and alkaline phosphatase (ALP) serum levels and pathological lesions in the liver. Abbas Alipourkabir et al., 2015, observed a significant increase in AST activity across all treatment groups. Additionally, while treatment with ZnO nanoparticles raised ALT activity in all groups, only the Nano ZnO 150mg/kg and Nano ZnO 200mg/kg doses resulted in a significant increase compared to the control group [45].

Alkaline Phosphatase (ALP) Levels: ALP levels were lower in the control group, with higher levels in the treated groups across all doses, further indicating liver dysfunction and potential biliary obstruction. This is consistent with the results of the pathotoxic study by Ghareeb et al, 2023 [46].

Thiobarbituric Acid Reactive Substances (TBARS) Concentration: In agreement with a previous study, our results showed induced lipid peroxidation. The control group had the lowest TBARS concentration, while higher levels in the treated groups suggest increased lipid peroxidation and oxidative stress in response to ZnO NP exposure [47].

Overall, these results demonstrate that chronic exposure to ZnO NPs induces significant biochemical alterations, reflecting liver damage, enhanced oxidative stress, and compromised antioxidant defenses. The dose-dependent effects underscore the potential health risks associated with prolonged exposure to ZnO nanoparticles.

The effects of ZnO nanoparticle exposure on various respiratory and Brain proteins and enzymes

Total Protein Content: The control group exhibited a total protein content of approximately 11 mg/ml, which serves as the baseline for normal conditions. In the low and middle chronic dose groups, the protein content remained relatively stable at around 10 and 11 mg/ml, respectively, indicating minimal impact at these doses. However, the high dose group showed a notable decrease to 9 mg/ml, suggesting that higher concentrations of ZnO nanoparticles may impair protein synthesis or promote protein degradation.

Acetylcholinesterase (AchE) Activity: AchE specific activity was significantly reduced in all ZnO nanoparticle-treated groups compared to the control group. The control group's activity was around 7 μmoles/min/mg protein, while the treated groups exhibited reduced activities of approximately 3, 4, and 3 μmoles/min/mg protein for the low, middle, and high doses, respectively.

This reduction indicates potential neurotoxicity, as AchE is crucial for synaptic transmission and its inhibition can lead to disrupted neuronal communication. This is in accordance with previous study stating ZnO NPs disturbed cholinergic neurotransmission in the hippocampus, which may potentially alter hippocampal synaptic plasticity or modulate cellular response [47].

Total Mitochondrial Protein Content: The control group had the highest total mitochondrial protein content at approximately 11 mg/ml. This level decreased in the treated groups, with the low, middle, and high dose groups showing levels of about 8, 7, and 8 mg/ml, respectively. The reduction in mitochondrial protein content suggests potential mitochondrial dysfunction or damage due to ZnO nanoparticle exposure, which could impair cellular energy metabolism. This could be explained by data from Kao et al. 2012 who hypothesized the mechanical toxicological pathway of ZnO nanoparticles. The entrance and dissolution of ZnO NPs in the cytosol cause an initial increase in cytosolic Zn^{2+} levels. The mitochondria then absorb the excess Zn^{2+}, leading to an elevated concentration of Zn^{2+} within the mitochondria. This high mitochondrial Zn^{2+} concentration induces the collapse of the mitochondrial membrane potential, which activates caspase-3, resulting in cell apoptosis and the release of lactate dehydrogenase (LDH) [49].

Na+/K+ ATPase Activity: Na+/K+ ATPase activity was significantly higher in the control group at approximately 33 nmole/ml. The treated groups exhibited decreased activities of around 24, 20, and 21 nmole/ml for the low, middle, and high doses, respectively. Similarly, Na+/K+ ATPase specific activity was highest in the control group at about 23 µmol Pi/mg protein/min, while the treated groups showed reduced specific activities of around 10, 12, and 16 µmol Pi/mg protein/min. This enzyme is vital for maintaining cellular ion balance and membrane potential; thus, its decreased activity indicates disrupted cellular homeostasis and potential cytotoxicity induced by ZnO nanoparticles. Previous data suggested that 10^{-4} g/ml nano-ZnO solution can lead to an enhancement in the current amplitudes of I_{Na} and I_K by increasing the opening number of sodium channels, delaying rectifier potassium channels, and enhancing the excitability of neurons, which lead to Na^+ influx and the accumulation of intracellular Na^+, as well as K^+ efflux plus the loss of cytoplasmic K^+. These may disturb the ionic homeostasis and the physiological functions of neurons [50].

These findings demonstrate that chronic exposure to ZnO nanoparticles leads to significant biochemical and enzymatic changes, particularly at higher doses. These alterations suggest potential toxic effects, including impaired protein synthesis, neurotoxicity, mitochondrial dysfunction, and disrupted ion balance, which may contribute to adverse health outcomes.

The impact of ZnO nanoparticle (ZnO NP) exposure on the expression levels of several key inflammatory and neurotransmission enzymes

For inducible nitric oxide synthase (iNOS), the control group exhibited a baseline expression level, while the treated groups showed a slight increase. This suggests that ZnO NP exposure may induce a mild inflammatory response, although the increase is not substantial. Previous studies have shown that treatment of the liver and kidney tissues with various concentrations of ZnO-NPs up-regulated the expression of this gene meaningfully ($p < 0.05$), ranging from 1.1 up to 3.9 folds. The up regulation of this gene confirmed the presence of inflammation in the mice kidney and liver treated with different concentrations of zinc nanoparticles [51].

Tyrosine hydroxylase (TH) expression levels were slightly higher in the treated groups compared to the control. As TH is a critical enzyme in the synthesis of catecholamines, this increase implies that ZnO NPs might enhance catecholamine production, potentially affecting neurotransmitter regulation [52].

Monocyte chemoattractant protein (MCP) expression was moderately elevated in the treated groups compared to the control. This suggests that ZnO NP exposure could promote the recruitment of monocytes, thereby enhancing inflammatory processes. MCP act as a secondary pro-inflammatory mediator that is typically induced by primary pro-inflammatory mediators such as interleukin-1 (IL-1) or tumor necrosis factor (TNF). Accumulating evidences suggest that MCP1 has the ability to compromise the integrity of BBB and modulate the progression of various diseases. Suzuki, Y., et al., 2014 reported that exposure to ZnO nanoparticles increased the level of monocyte chemotactic protein-1 (MCP-1) and induced the migration of THP-1 monocyte mediated by increased MCP-1 [54].

Conversely, the expression levels of vesicular monoamine transporter (VMAT) were lower in the treated groups. VMAT is crucial for the transport and storage of neurotransmitters in vesicles, and its reduced expression indicates that ZnO NP exposure might impair these processes, potentially disrupting normal neurotransmission [55].

Overall, these findings indicate that chronic exposure to ZnO NPs can induce mild inflammatory responses and alter neurotransmitter synthesis and storage. The dose-dependent changes

in expression levels underscore the potential neurotoxic effects of ZnO NPs, highlighting the need for careful consideration of their use and exposure limits to mitigate potential health risks.

5. Conclusion

The investigation into the effects of zinc oxide nanoparticles (ZnO NPs) highlights their significant potential in nanomedicine, contrasted with notable health and environmental risks. While ZnO NPs offer promising applications in medical imaging, drug delivery, and antiviral prophylaxis, they also pose potential neurotoxic effects by traversing biological barriers and accumulating in sensitive organs like the brain.

Our study demonstrated that chronic exposure to ZnO NPs induces mild inflammatory responses, as evidenced by increased iNOS and MCP expression, and potential neurotoxicity indicated by reduced acetylcholinesterase (AchE) activity and impaired neurotransmitter storage. Additionally, significant changes in enzyme activities and protein content suggest mitochondrial dysfunction and disrupted cellular ion balance.

Hematological evaluations revealed dose-dependent hematotoxicity, with higher doses causing robust inflammatory responses and compromised red blood cell integrity. These findings underscore the importance of understanding ZnO NP-induced toxicity mechanisms.

Overall, the dose-dependent effects observed necessitate cautious application and rigorous regulation of ZnO NPs to mitigate health risks. Balancing their promising applications with thorough safety assessments is crucial to protect human health and the environment. Further research is needed to elucidate the full spectrum of ZnO NP effects and develop guidelines for their safe and effective use.

References

1. Han D, Tian Y, Zhang T, Ren G, Yang Z. Nano-zinc oxide damages spatial cognition capability via over-enhanced long-term potentiation in hippocampus of Wistar rats. Int J Nanomedicine. 2011;6:1453.https://doi.org/10.2147/IJN.S18507

2. Mousa AB, Moawad R, Abdallah Y, Abdel-Rasheed M, Zaher AM. Zinc oxide nanoparticles promise anticancer and antibacterial activity in ovarian cancer. Pharm Res. 2023 Oct;40(10):2281-90.https://doi.org/10.1007/s11095-023-03505-0

3. De Jong WH, Borm PJ. Drug delivery and nanoparticles: applications and hazards. Int J Nanomedicine. 2008;3(2):133. https://doi.org/10.2147/IJN.S596

4. Chang YN, Zhang M, Xia L, Zhang J, Xing G. The toxic effects and mechanisms of CuO and ZnO nanoparticles. Materials. 2012;5(12):2850-71. https://doi.org/10.3390/ma5122850

5. Yang Z, Liu ZW, Allaker RP, Reip P, Oxford J, Ahmad Z, Reng G. A review of nanoparticle functionality and toxicity on the central nervous system. In: Nanotechnology, the Brain, and the Future. Springer; 2013. p. 313-32. https://doi.org/10.1007/978-94-007-1787-9_18

6. Sruthi S, Ashtami J, Mohanan PV. Biomedical application and hidden toxicity of Zinc oxide nanoparticles. Materials Today Chemistry. 2018 Dec 1;10:175-86. https://doi.org/10.1016/j.mtchem.2018.09.008

7. Benarroch EE. Na+, K+-ATPase functions in the nervous system and involvement in neurologic disease. Neurology. 2011;76(3):287-93. https://doi.org/10.1212/WNL.0b013e3182074c2f

8. Mavelli I, Rigo A, Federico R, Ciriolo M, Rotilio G. Superoxide dismutase, glutathione peroxidase and catalase in developing rat brain. Biochem J. 1982;204(2):535-40. https://doi.org/10.1042/bj2040535

9. Keller JN, Kindy MS, Holtsberg FW, Clair D, Yen H, Germeyer A, Steiner SM, Bruce-Keller AJ, Hutchins JB, Mattson MP. Mitochondrial manganese superoxide dismutase prevents neural apoptosis and reduces ischemic brain injury: suppression of peroxynitrite production, lipid peroxidation, and mitochondrial dysfunction. J Neurosci. 1998;18(2):687-97. https://doi.org/10.1523/JNEUROSCI.18-02-00687.1998

10. Mahjoubian M, Naeemi AS, Moradi-Shoeili Z, Tyler CR, Mansouri B. Oxidative stress, genotoxic effects, and other damages caused by chronic exposure to silver nanoparticles (Ag NPs) and zinc oxide nanoparticles (ZnO NPs), and their mixtures in zebrafish (Danio rerio). Toxicol Appl Pharmacol. 2023;472:116569. https://doi.org/10.1016/j.taap.2023.116569

11. Lowry OH, Rosebrough NJ, Farr AL, Randall RJ. Protein measurement with the Folin phenol reagent. J Biol Chem. 1951;193(1):265-75. https://doi.org/10.1016/S0021-9258(19)52451-6

12. Rahman M, Wang J, Patterson TA, Saini UT, Robinson BL, Newport GD, Murdock RC, Schlager JJ, Hussain SM, Ali SF. Expression of genes related to oxidative stress in the mouse brain after exposure to silver-25 nanoparticles. Toxicol Lett. 2009;187(1):15-21. https://doi.org/10.1016/j.toxlet.2009.01.020

13. Reitman S, Frankel S. A colorimetric method for the determination of serum glutamic oxalacetic and glutamic pyruvic transaminases. Am J Clin Pathol. 1957;28(1):56-63. https://doi.org/10.1093/ajcp/28.1.56

14. Belfield A, Goldberg D. Revised assay for serum phenyl phosphatase activity using 4-amino-antipyrine. Enzyme. 1970;12(5):561-73. https://doi.org/10.1159/000459586

15. Ellman GL, Courtney KD, Andres V, Featherstone RM. A new and rapid colorimetric determination of acetylcholinesterase activity. Biochem Pharmacol. 1961;7(2):88-95. https://doi.org/10.1016/0006-2952(61)90145-9

16. Koch R. Chlorinated hydrocarbon insecticides: Inhibition of rabbit brain ATPase activities. J Neurochem. 1969;16(2):269-71. https://doi.org/10.1111/j.1471-4159.1969.tb05944.x

17. Taussky HH, Shorr E. A microcolorimetric method for the determination of inorganic phosphorus. J Biol Chem. 1953;202(2):675-85. https://doi.org/10.1016/S0021-9258(18)66180-0

18. Habig WH, Pabst MJ, Jakoby WB. Glutathione S-transferases: the first enzymatic step in mercapturic acid formation. J Biol Chem. 1974;249(22):7130-9. https://doi.org/10.1016/S0021-9258(19)42083-8

19. Beutler E, Duron O, Kelly BM. Improved method for the determination of blood glutathione. J Lab Clin Med. 1963;61:882-8.

20. Aebi H. Catalase in vitro. Methods Enzymol. 1984;105:121-6. https://doi.org/10.1016/S0076-6879(84)05016-3

21. Fossati P, Prencipe L, Berti G. Use of 3,5-dichloro-2-hydroxybenzenesulfonic acid/4-aminophenazone chromogenic system in direct enzymic assay of uric acid in serum and urine. Clin Chem. 1980;26(2):227-31. https://doi.org/10.1093/clinchem/26.2.0227

22. Paglia DE, Valentine WN. Studies on the quantitative and qualitative characterization of erythrocyte glutathione peroxidase. Transl Res. 1967;70(1):158-69.

23. Tappel A, Zalkin H. Inhibition of lipide peroxidation in mitochondria by vitamin E. Arch Biochem Biophys. 1959;80(2):333-6. https://doi.org/10.1016/0003-9861(59)90258-9

24. Tienes BM, Perkins RJ, Shoemaker RK, Dukovic G. Layered phosphonates in colloidal synthesis of anisotropic ZnO nanocrystals. Chem Mater. 2013;25:4321-9. doi: 10.1021/cm402465w. https://doi.org/10.1021/cm402465w

25. Shen ZC, Zhou HJ, Chen HY, Xu H, Feng CH, Zhou XH. Synthesis of nano-zinc oxide loaded on mesoporous silica by coordination effect and its photocatalytic degradation property of methyl orange. Nanomater-Basel. 2018;8:317. doi: 10.3390/nano8050317. https://doi.org/10.3390/nano8050317

26. Goh EG, Xu X, McCormick PG. Effect of particle size on the UV absorbance of zinc oxide nanoparticles. Scripta Mater. 2014;78:49-52. doi: 10.1016/j.scriptamat.2014.01.033. https://doi.org/10.1016/j.scriptamat.2014.01.033

27. Ji XH, Song XL, Li J, Bai YB, Yang WS, Peng XG. Size control of gold nanocrystals in citrate reduction: the third role of citrate. J Am Chem Soc. 2007;129:13939-48. doi: 10.1021/ja074447k. https://doi.org/10.1021/ja074447k

28. Chen YF, Johnson E, Peng XG. Formation of monodisperse and shape-controlled MnO nanocrystals in non-injection synthesis: self-focusing via ripening. J Am Chem Soc. 2007;129:10937-47. doi: 10.1021/ja073023n. https://doi.org/10.1021/ja073023n

29. Fan ZY, Lu JG. Zinc oxide nanostructures: synthesis and properties. J Nanosci Nanotechnol. 2005;5:1561-73. doi: 10.1166/jnn.2005.182. https://doi.org/10.1166/jnn.2005.182

30. Cao D, Gong S, Shu X, Zhu D, Liang S. Preparation of ZnO nanoparticles with high dispersibility based on oriented attachment (OA) process. Nanoscale Res Lett. 2019 Dec;14(1):210. https://doi.org/10.1186/s11671-019-3038-3

31. Sruthi S, Ashtami J, Mohanan PV. Biomedical application and hidden toxicity of Zinc oxide nanoparticles. Materials Today Chemistry. 2018 Dec 1;10:175-86. https://doi.org/10.1016/j.mtchem.2018.09.008

32. Attia H, Nounou H, Shalaby M. Zinc oxide nanoparticles induced oxidative DNA damage, inflammation and apoptosis in rat's brain after oral exposure. Toxics. 2018 May 26;6(2):29. https://doi.org/10.3390/toxics6020029

33. Hersh AM, Alomari S, Tyler BM. Crossing the blood-brain barrier: advances in nanoparticle technology for drug delivery in neuro-oncology. Int J Mol Sci. 2022 Apr 9;23(8):4153. https://doi.org/10.3390/ijms23084153

34. Singh R, Cheng S, Singh S. Oxidative stress-mediated genotoxic effect of zinc oxide nanoparticles on Deinococcus radiodurans. 3 Biotech. 2020 Feb;10(2):66. https://doi.org/10.1007/s13205-020-2054-4

35. Olufunmilayo EO, Gerke-Duncan MB, Holsinger RD. Oxidative stress and antioxidants in neurodegenerative disorders. Antioxidants. 2023 Feb 18;12(2):517. https://doi.org/10.3390/antiox12020517

36. Hong JS, Park MK, Kim MS, Lim JH, Park GJ, Maeng EH, Shin JH, Kim YR, Kim MK, Lee JK, Park JA. Effect of zinc oxide nanoparticles on dams and embryo-fetal development in rats. Int J Nanomedicine. 2014 Dec 15;9(Suppl 2):145-57. https://doi.org/10.2147/IJN.S57931

37. Susilo A, AbdulHussein AH, Abed Hussein S, Kamal M, Jawad Alnaja M, Hussein Kareem A, Talib HA, B Sapayev I, Suvonova L. Evaluating the Hematological Impact of Zinc Oxide Nanoparticles in NMRI Mice: An In Vivo Analysis. Bioinorganic Chemistry and Applications. 2023 Jul 18;2023.

38. Zhu X, Hondow NS, Muskens OL, Evans SD. High-resolution detection of DNA-linked nanoparticles and their diffusion properties in solution via wide-field photon counting. Nano Lett. 2022 Dec 8;22(23):9447-54.

39. Czyżowska A, Barbasz A. A review: zinc oxide nanoparticles-friends or enemies?. Int J Environ Health Res. 2022 Apr 3;32(4):885-901. https://doi.org/10.1080/09603123.2020.1805415

40. Pandurangan M, Veerappan M, Kim DH.

Cytotoxicity of zinc oxide nanoparticles on antioxidant enzyme activities and mRNA expression in the cocultured C2C12 and 3T3-L1 cells. Appl Biochem Biotechnol. 2015;175(3):1270-80. https://doi.org/10.1007/s12010-014-1351-y

41. Trevisan R, Delapedra G, Mello DF, Arl M, Schmidt ÉC, Meder F, et al. Gills are an initial target of zinc oxide nanoparticles in oysters Crassostrea gigas, leading to mitochondrial disruption and oxidative stress. Aquat Toxicol. 2014;153:27-38. https://doi.org/10.1016/j.aquatox.2014.03.018

42. Akhtar MJ, Ahamed M, Kumar S, Khan MM, Ahmad J, Alrokayan SA. Zinc oxide nanoparticles selectively induce apoptosis in human cancer cells through reactive oxygen species. Int J Nanomedicine. 2012;7:845-57. https://doi.org/10.2147/IJN.S29129

43. Sharma V, Singh P, Pandey AK, Dhawan A. Induction of oxidative stress, DNA damage and apoptosis in mouse liver after sub-acute oral exposure to zinc oxide nanoparticles. Mutat Res Genet Toxicol Environ Mutagen. 2012;745(1-2):84-91. https://doi.org/10.1016/j.mrgentox.2011.12.009

44. Sharma A, Mishra A, Chhabra M. Rapid measurement of bacterial contamination in water: A catalase responsive-electrochemical sensor. Heliyon. 2024 Mar 15;10(5). https://doi.org/10.1016/j.heliyon.2024.e26724

45. Abbasalipourkabir R, Moradi H, Zarei S, Asadi S, Salehzadeh A, Ghafourikhosroshahi A, et al. Toxicity of zinc oxide nanoparticles on adult male Wistar rats. Food Chem Toxicol. 2015;84:154-60. https://doi.org/10.1016/j.fct.2015.08.019

46. Ghareeb OA, Ali QA. Pathotoxic Impact of Zinc Oxide Nanoparticles on Liver Function and Protective Role of Silymarin. Curr Innov Dis Health Res. 2023 Jul 24;3:153-61. https://doi.org/10.9734/bpi/cidhr/v3/10703F

47. Mirzaei F, Abbasi E, Mirzaei A, Hosseini NF, Naseri N, Khodadadi I, et al. Toxicity and hepatoprotective effects of ZnO nanoparticles on normal and high-fat diet-fed rat livers: mechanism of action. Biol Trace Elem Res. 2024 Mar 5:1-9. https://doi.org/10.1007/s12011-024-04108-5

48. Guo Z, Zhang P, Luo Y, Xie HQ, Chakraborty S, Monikh FA, et al. Intranasal exposure to ZnO nanoparticles induces alterations in cholinergic neurotransmission in rat brain. Nano Today. 2020 Dec 1;35:100977. https://doi.org/10.1016/j.nantod.2020.100977

49. Kao Y, Chen Y, Cheng T, Chiung Y, Liu P. Zinc oxide nanoparticles interfere with zinc ion homeostasis to cause cytotoxicity. Toxicol Sci. 2012;125(2):462-72. https://doi.org/10.1093/toxsci/kfr319

50. Zhao J, Xu L, Zhang T, Ren G, Yang Z. Influences of nanoparticle zinc oxide on acutely isolated rat hippocampal CA3 pyramidal neurons. Neurotoxicology. 2009;30(2):220-30. https://doi.org/10.1016/j.neuro.2008.12.005

51. Rahimi G, Shah-Mohammad K, Zarei M, Shokoohi M, Oskoueian E, Moghaddam-Poorbagher MR, et al. Zinc oxide nanoparticles synthesized using Hyssopus Officinalis L. Extract Induced oxidative stress and changes the expression of key genes involved in inflammatory and antioxidant systems. Biol Res. 2022;55. https://doi.org/10.1186/s40659-022-00392-4

52. Johnson ME, Salvatore MF, Maiolo SA, Bobrovskaya L. Tyrosine hydroxylase as a sentinel for central and peripheral tissue responses in Parkinson's progression: Evidence from clinical studies and neurotoxin models. Prog Neurobiol. 2018 Jun 1;165:1-25. https://doi.org/10.1016/j.pneurobio.2018.01.002

53. Bernardino PN, Luo AS, Andrew PM, Unkel CM, Gonzalez MI, Gelli A, et al. Evidence implicating blood-brain barrier impairment in the pathogenesis of acquired epilepsy following acute organophosphate intoxication. J Pharmacol Exp Ther. 2024;388(2):301-12. https://doi.org/10.1124/jpet.123.001836

54. Suzuki Y, Tada-Oikawa S, Ichihara G, Yabata MI, Izuoka K, Suzuki M, et al. Zinc oxide nanoparticles induce migration and adhesion of monocytes to endothelial cells and accelerate foam cell formation. Toxicol Appl Pharmacol. 2014;278(1):16-25. https://doi.org/10.1016/j.taap.2014.04.010

55. Alwindi M, Bizanti A. Vesicular monoamine transporter (VMAT) regional expression and roles in pathological conditions. Heliyon. 2023 Nov 15. https://doi.org/10.1016/j.heliyon.2023.e22413